

Air Force Institute of Technology

**AFIT Scholar**

---

Faculty Publications

---

2022

## Magneto-Exothermic Catalytic Chemical Reaction along a Curved Surface

Muhammad Ashraf

Uzma Ahmad

Saqib Zia

Rama S. R. Gorla

*Air Force Institute of Technology*

Amnah S. Al-Johani

*See next page for additional authors*

Follow this and additional works at: <https://scholar.afit.edu/facpub>



Part of the [Electromagnetics and Photonics Commons](#), and the [Other Mechanical Engineering Commons](#)

---

### Recommended Citation

Muhammad Ashraf, Uzma Ahmad, Saqib Zia, Rama Suba Reddy Gorla, Amnah S. Al-Johani, Ilyas Khan, Mulugeta Andualem, "Magneto-Exothermic Catalytic Chemical Reaction along a Curved Surface", *Mathematical Problems in Engineering*, vol. 2022, Article ID 8439659, 10 pages, 2022. <https://doi.org/10.1155/2022/8439659>

This Article is brought to you for free and open access by AFIT Scholar. It has been accepted for inclusion in Faculty Publications by an authorized administrator of AFIT Scholar. For more information, please contact [richard.mansfield@afit.edu](mailto:richard.mansfield@afit.edu).



---

**Authors**

Muhammad Ashraf, Uzma Ahmad, Saqib Zia, Rama S. R. Gorla, Amnah S. Al-Johani, Ilyas Khan, and Mulugeta Andualem

## Research Article

# Magneto-Exothermic Catalytic Chemical Reaction along a Curved Surface

Muhammad Ashraf,<sup>1</sup> Uzma Ahmad,<sup>1</sup> Saqib Zia,<sup>2</sup> Rama Suba Reddy Gorla,<sup>3</sup>  
Annah S. Al-Johani,<sup>4</sup> Ilyas Khan ,<sup>5</sup> and Mulugeta Andualem <sup>6</sup>

<sup>1</sup>Department of Mathematics, Faculty of Science, University of Sargodha, Sargodha 40100, Pakistan

<sup>2</sup>Department of Mathematics, COMSATS University Islamabad, Islamabad 44000, Pakistan

<sup>3</sup>Department of Aeronautics and Astronautics, Air Force Institute of Technology, Wright Patterson Air Force Base, Dayton, OH 45433, USA

<sup>4</sup>Mathematics Department, Faculty of Science, University of Tabuk, Tabuk, Saudi Arabia

<sup>5</sup>Department of Mathematics, College of Science Al-Zulfi, Majmaah University, Al-Majmaah 11952, Saudi Arabia

<sup>6</sup>Department of Mathematics, Bonga University, Bonga, Ethiopia

Correspondence should be addressed to Mulugeta Andualem; [mulugetaandualem4@gmail.com](mailto:mulugetaandualem4@gmail.com)

Received 29 October 2021; Accepted 25 March 2022; Published 9 May 2022

Academic Editor: Muhammad Afzal Rana

Copyright © 2022 Muhammad Ashraf et al. This is an open access article distributed under the Creative Commons Attribution License, which permits unrestricted use, distribution, and reproduction in any medium, provided the original work is properly cited.

In the current study, the physical behavior of the boundary layer flows along a curved surface owing exothermic catalytic chemical reaction, and the magnetic field is investigated. The mathematical model comprised of a part of momentum, energy, and mass equations, which are solved using a finite difference method along with primitive variable formulation. Numerical solutions, using the method of quantitative differentiation, are made with the appropriate choice of dimensionless parameters. Analysis of the results obtained shows that the field temperature and flow of fluids are strongly influenced by the combined effects of catalytic chemical reactions and the magnetic field. The effects of skin friction, heat transfer, mass transfer, mass concentration, and temperature distribution along the curved surface are illustrated in the plots and in the form of tables. By setting the controlling parameters at the boundaries, the boundary conditions at the surface and away from the surface are determined in each graph. With a larger range of body shape parameter  $n$ , skin friction and heat transfer are improved, but mass transfer is reduced. Due to the increasing values of the exothermic parameter, the fluid velocity and mass concentration are decreased gradually and the temperature distribution is increased dramatically.

## 1. Introduction

A mechanism that occurs due to temperature fluctuations because of the temperature difference is known as natural convection. The integrated approach to evolutionary and chemical reactions is embedded in both exploratory research and theoretical diversity and flow patterns due to its wide range of engineering and industrial applications. Natural convection has many applications in terms of temperature, solar energy, and dispersion of chemical pollutants, chemical catalytic reactors, and pottery. However, the combined process of natural convection flow and exothermic catalytic chemical reaction and the incorporation of magnetohydrodynamic into the

curved area have not yet been investigated by researchers. The contributions of the research community to these approaches are highlighted below.

Magnetohydrodynamic (MHD) -free convection boundary layer flow of an incompressible steady viscous and electrically conducting fluid with uniform mass and heat flux in the presence of strong cross magnetic field along a vertical flat heated plate was studied by D'sa [1]. Kuiken [2] investigated the problem of magnetohydrodynamic-free convection of an electrically conducting fluid in a strong cross field. He highlighted the important cases of both the liquid metals and ionized gases. Hossain et al. [3] considered the MHD natural convection flow along a vertical porous plate in the presence of

variable magnetic field. The combined mechanism of magnetic field and chemical reaction for natural convection flow over a stretching sheet was investigated by Affify [4]. Later, Makinde and Aziz [5] numerically studied the mechanism of heat and mass transfer from a vertical plate embedded in a perforated area by taking into account the chemical reaction and the magnetic field. The study of MHD two immiscible fluids present between the isothermal and insulated moving plates was carried out by Stamenković et al. [6]. Ashraf et al. [7] studied the combined effects of synthetic and radiation in the natural convection flow past the permissible magnetic plate. Rongy [8] addressed that intense changes occur in the exothermic autocatalytic front that is generating in the presence of Marangoni flows. Rout et al. [9] considered the simultaneous heat transfer over a straight moving plate to quantify the combined effects of chemical reactions and thermal production on static boundary conditions. Numerical studies on the reaction of exothermic/endothermic chemicals and the ability to regenerate Arrhenius in MHD-free convection flow by meeting the effects of radiation were performed by Maleque [10]. Later, he studied the engineering of the binary chemical reaction associated with the natural MHD flow of convection over an accessible plate in [11]. The study on production of heat due to exothermic reaction in a fully developed electrically conducting mixed convection flow was carried out by Jayabalan et al. [12].

Ashraf et al. [13] proposed a model of mixed convective flow in a specific magnetic field to study the effects of thermal conductivity and viscosity that vary in temperature. Anwar et al. [14, 15] introduced the heat transfer and Joule heating in a magnetized flow model. Daniel et al. [16] analyzed the flow of MHD radiations to discuss the effects of nanofluid formation on an expanded sheet with a flexible layer. The transcendent and stable natural flow of hot liquid in a vertical station considering the conditions of slipperiness and temperature of the Newtonian was investigated by Hamza [17]. The chemical reaction that causes heat dissipation was considered obtained by computer analysis of free-flow convection in a curved area by Ashraf et al. [18].

## 2. Governing Mathematical Model and Coordinate System

Consider a steady and two-dimensional natural convective flow in the presence of chemical reaction on a curved surface, as shown in Figure 1. A nondimensional Cartesian coordinate system is taken along and normal to the curved surface, respectively. Here, surface temperature is assumed to be greater than the ambient temperature. Moreover, the gravitational acceleration  $g_x$  is acting parallel to the curved surface,  $r(z)$  is a fixed side, and  $dr/dz = 0$  indicates that there is no fluid flow along  $r(z)$ , thus representing an external flow. Considering the above all assumptions, the dimensionless transport boundary layer equations for two-dimensional steady electrically conducting and incompressible natural convection flow of along a curved surface in the presence of exothermic binary chemical reaction (by following Ashraf et al. [18]) are,  $\mathbf{dr}/\mathbf{dz} = 0$ .

With all the above assumptions, the dimensionless transport boundary layer equations for natural convection flow driven along the curved surface are

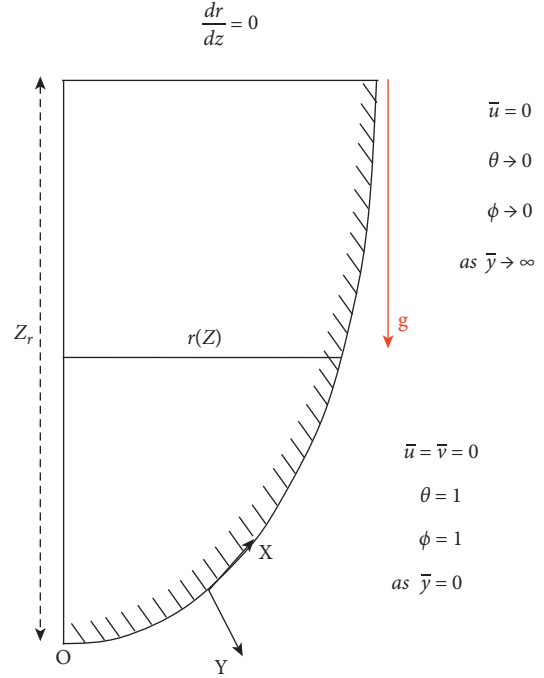


FIGURE 1: Flow analysis driven along the curved surface.

$$\frac{\partial \bar{u}}{\partial \bar{x}} + \frac{\partial \bar{v}}{\partial \bar{y}} = 0, \quad (1)$$

$$\bar{u} \frac{\partial \bar{u}}{\partial \bar{x}} + \bar{v} \frac{\partial \bar{u}}{\partial \bar{y}} + \frac{\bar{u}^2}{2\bar{x}} (P(\bar{x}) + Q(\bar{x})) = \frac{\partial^2 \bar{u}}{\partial \bar{y}^2} + \theta + \phi - M\bar{u}, \quad (2)$$

$$\bar{u} \frac{\partial \theta}{\partial \bar{x}} + \bar{v} \frac{\partial \theta}{\partial \bar{y}} = \frac{1}{\text{Pr}} \frac{\partial^2 \theta}{\partial \bar{y}^2} + \beta \lambda^2 (1 + n\gamma\theta) \exp\left(\frac{-E}{1 + \gamma\theta}\right) \theta, \quad (3)$$

$$\bar{u} \frac{\partial \phi}{\partial \bar{x}} + \bar{v} \frac{\partial \phi}{\partial \bar{y}} = \frac{1}{\text{Sc}} \frac{\partial^2 \phi}{\partial \bar{y}^2} + \lambda^2 (1 + n\gamma\theta) \exp\left(\frac{-E}{1 + \gamma\theta}\right) \phi.$$

The dimensionless variables used in the above equations are

$$\begin{aligned} \bar{x} &= \frac{x}{l}, \\ \bar{y} &= \frac{y \text{Gr}^{-1/4}}{l}, \\ u &= U_s \bar{u}, \\ v &= U_s \frac{\text{Gr}^{-1/4}}{\bar{v}}, \\ \text{Gr} &= \frac{g_x \beta \Delta T l^3}{\nu^2}, \\ \theta &= T - \frac{T_\infty}{T_w} - T_\infty, \\ \phi &= C - \frac{C_\infty}{C_w} - C_\infty, \end{aligned} \quad (4)$$

where  $U_s = (g_x \beta T_s l) / 2$  is the velocity scale defined in Ashraf et al. [18]. In the above equations,  $\text{Pr} = \nu/\alpha$ ,  $\text{Sc} = \nu/D_B$ , and  $M = \sigma B_0^2 l / \rho U_s$  are Prandtl, Schmidt, and Hartmann

numbers, respectively. Here,  $\beta$  is the exothermic parameter,  $\lambda^2 = K_r^2 l / U_s$  is the dimensionless chemical reaction rate constant, where  $k_r^2$  is the chemical reaction rate constant and  $l$  is the characteristic length. The symbol,  $\gamma = T_w - T_\infty / T_\infty$ , is the temperature relative parameter, and  $E = E_a / k T_\infty$  is the dimensionless activation energy, with  $E_a$  as the activation energy and  $k = 1.380649 \times 10^{-23} \text{JK}^{-1}$  is the Boltzman constant. The notations  $P(\bar{x})$  denotes the wall temperature function and  $Q(\bar{x})$  represents the body shape function which are defined as (see details in Ashraf et al. [18])

$$P(\bar{x}) = \frac{d \ln T_w}{d \ln \bar{x} l}, \quad (5)$$

$$Q(\bar{x}) = \frac{d \ln g_x}{d \ln \bar{x} l},$$

where  $g_x$  is the acceleration due to gravity along the surface, and it is defined as

$$\bar{u} = 0, \bar{v} = 0, \theta = 1, \phi = 1 \text{ at } \bar{y} = 0, \quad (6)$$

which subjected to the boundary conditions which are

$$\bar{u} = 0, \theta \rightarrow 0, \phi \rightarrow 0 \text{ as } \bar{y} \rightarrow \infty. \quad (7)$$

By following Ashraf et al. [18], it is noted that equation (2) is in a simple form that can be solved numerically for any values of  $P(\bar{x})$  and  $Q(\bar{x})$ . Thus, the conservation equations along with boundary conditions (by dropping bars) take the following form:

$$\frac{\partial u}{\partial x} + \frac{\partial v}{\partial y} = 0, \quad (8)$$

$$u \frac{\partial u}{\partial x} + v \frac{\partial u}{\partial y} + \tilde{n} \frac{u^2}{2x} = \frac{\partial^2 u}{\partial y^2} + \theta + \phi - \text{Mu}, \quad (9)$$

$$u \frac{\partial \theta}{\partial x} + v \frac{\partial \theta}{\partial y} = \frac{1}{\text{Pr}} \frac{\partial^2 \theta}{\partial y^2} + \beta \lambda^2 (1 + n\gamma\theta) \exp\left(\frac{-E}{1 + \gamma\theta}\right) \theta, \quad (10)$$

$$u \frac{\partial \phi}{\partial x} + v \frac{\partial \phi}{\partial y} = \frac{1}{\text{Sc}} \frac{\partial^2 \phi}{\partial y^2} + \lambda^2 (1 + n\gamma\theta) \exp\left(\frac{-E}{1 + \gamma\theta}\right) \phi, \quad (11)$$

under dimensionless boundary conditions:

$$\begin{aligned} u = 0, v = 0, \theta = 1, \phi = 1 \text{ at } y = 0, \\ u = 0, \theta \rightarrow 0, \phi \rightarrow 0 \text{ as } y \rightarrow \infty. \end{aligned} \quad (12)$$

### 3. Solution Methodology

Before applying the finite difference method (FDM) used by Ashraf et al. [18] and many other, for the proposed dimensionless model presented in equations (8)–(11) along with boundary conditions (12), it is first transformed into a convenient form by applying primitive variable formulation (PVF) to make the algorithm smooth. Then, the dimensionless transformed model is discretized by using a finite difference scheme. The central difference scheme is used along  $y$ -direction and the backward difference scheme is used along  $x$ -direction. To transform the above system of

equation into a primitive form, we use the following transformation:

$$\begin{aligned} u = x^{1/2} U(X, Y), v = x^{-1/4} V(X, Y), x = X, y = x^{1/4} Y, \\ \theta = \Theta(X, Y), \phi = \Phi(X, Y). \end{aligned} \quad (13)$$

By using (8) into equations (8)–(12), we have

$$\frac{U}{2} + X \frac{\partial U}{\partial X} - \frac{Y \partial U}{4 \partial Y} + \frac{\partial V}{\partial Y} = 0, \quad (14)$$

$$\left[\frac{1}{2} + \frac{\tilde{n}}{2}\right] U^2 + XU \frac{\partial U}{\partial X} + \left(V - \frac{YU}{4}\right) \frac{\partial U}{\partial Y} = \frac{\partial^2 U}{\partial Y^2} + \Theta + \Phi - \text{MX}^{1/2} U, \quad (15)$$

$$XU \frac{\partial \Theta}{\partial X} + \left(V - \frac{YU}{4}\right) \frac{\partial \Theta}{\partial Y} = \frac{1}{\text{Pr}} \frac{\partial^2 \Theta}{\partial Y^2} + \beta \lambda^2 (1 + n\gamma\Theta) \exp\left(\frac{-E}{1 + \gamma\Theta}\right) \Theta, \quad (16)$$

$$XU \frac{\partial \Phi}{\partial X} + \left(V - \frac{YU}{4}\right) \frac{\partial \Phi}{\partial Y} = \frac{1}{\text{Sc}} \frac{\partial^2 \Phi}{\partial Y^2} + \lambda^2 (1 + n\gamma\Theta) \exp\left(\frac{-E}{1 + \gamma\Theta}\right) \Phi. \quad (17)$$

The transformed boundary conditions are

$$\begin{aligned} U = 0, V = 0, \Theta = 1, \Phi = 1 \text{ at } Y = 0, \\ U = 0, \Theta \rightarrow 0, \Phi \rightarrow 0 \text{ as } Y \rightarrow \infty. \end{aligned} \quad (18)$$

**3.1. Discretization.** Equations (14)–(18) are solved with the help of a finite difference scheme. The derivative terms involved in these equations are transformed into convenient form by using difference formulation. The whole discretization process is given below:

$$\begin{aligned} \frac{\partial U}{\partial X} &= \frac{U_{i,j} - U_{i-1,j}}{\Delta X}, \frac{\partial U}{\partial Y} = \frac{U_{i+1,j} - U_{i-1,j}}{2\Delta Y}, \frac{\partial^2 U}{\partial Y^2} \\ &= \frac{U_{i-1,j} - 2U_{i,j} + U_{i+1,j}}{\Delta Y^2}. \end{aligned} \quad (19)$$

Here, the subscripts  $i$  and  $j$  are the unit vectors along and perpendicular to the surface, respectively. Using (11) into equations (14)–(17), we obtain a tridiagonal matrix which is then solved with the Gaussian elimination technique. The system of algebraic equations subjected to the boundary conditions (18) is given below:

$$\begin{aligned} V_{i+1,j} &= V_{i-1,j} - \Delta Y U_{i,j} - 2 \frac{\Delta Y}{\Delta X} X_i (U_{i,j} - U_{i-1,j}) \\ &\quad + \frac{Y_j}{4} (U_{i+1,j} - U_{i-1,j}), \\ \left. \begin{aligned} \mathbf{A}_1 U_{i-1,j} + \mathbf{B}_1 U_{i,j} + \mathbf{C}_1 U_{i+1,j} &= \mathbf{D}_1 \\ \mathbf{A}_2 \Theta_{i-1,j} + \mathbf{B}_2 \Theta_{i,j} + \mathbf{C}_2 \Theta_{i+1,j} &= \mathbf{D}_2 \\ \mathbf{A}_3 \Phi_{i-1,j} + \mathbf{B}_3 \Phi_{i,j} + \mathbf{C}_3 \Phi_{i+1,j} &= \mathbf{D}_3 \end{aligned} \right\}, \end{aligned} \quad (20)$$

where  $\mathbf{A}_k$ ,  $\mathbf{B}_k$ , and  $\mathbf{C}_k$  ( $k = 1, 2, 3$ ) are the coefficient matrices and  $\mathbf{D}_1$ ,  $\mathbf{D}_2$ ,  $\mathbf{D}_3$  are the column vectors for the unknown variables  $U$ ,  $\theta$ , and  $\Phi$ . The discretized boundary conditions are

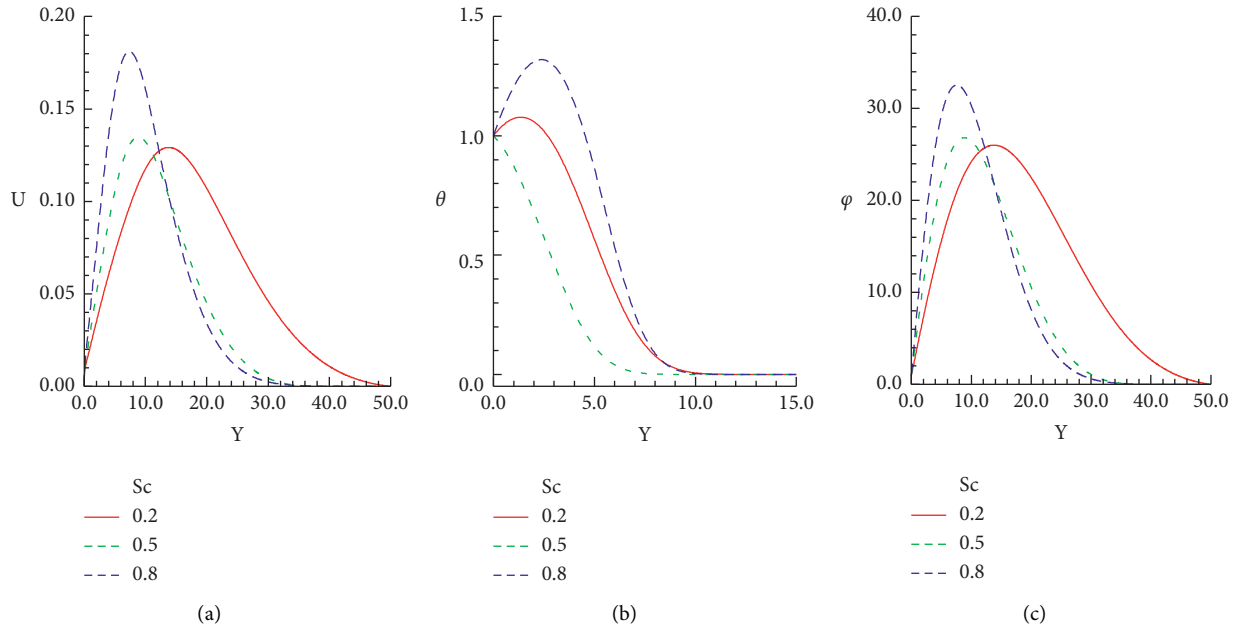


FIGURE 2: Plots for (a)  $U$ , (b)  $\theta$ , and (c)  $\phi$  for different choice of Schmidt number  $Sc$  when  $n = 0.3$ ,  $Pr = 7.0$ ,  $E = 0.8$ ,  $\beta = 0.1$ ,  $\gamma = 0.001$ ,  $M = 0.2$ , and  $\lambda = 0.5$ .

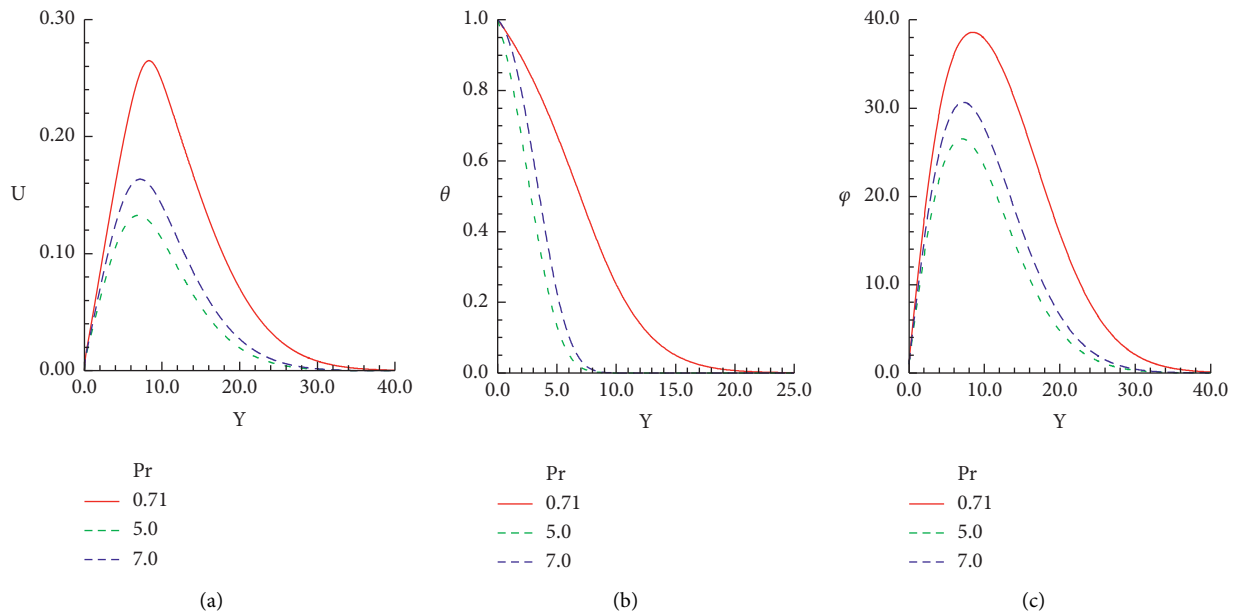


FIGURE 3: Plots for (a)  $U$ , (b)  $\theta$ , and (c)  $\phi$  for different choices of Prandtl number  $Pr$  when  $n = 0.3$ ,  $Sc = 0.8$ ,  $E = 0.8$ ,  $\beta = 0.001$ ,  $\gamma = 0.001$ ,  $M = 0.2$ , and  $\lambda = 0.5$ .

$$\begin{aligned} U_{i,j} = 0, V_{i,j} = 0, \theta_{i,j} = 1, \Phi_{i,j} = 1 \text{ at } Y_j = 0, \\ U_{i,j} = 0, \theta_{i,j} \longrightarrow 0, \Phi_{i,j} \longrightarrow 0 \text{ as } Y_j \longrightarrow \infty. \end{aligned} \quad (21)$$

Furthermore, the above system of equations given in (12) is solved by using Gaussian elimination technique. With the help of this technique, we determine the quantities  $U$ ,  $V$ ,  $\theta$ , and  $\Phi$ . Moreover, skin friction and rate of heat and mass transfer along the curved surface can be computed by using the following laws:

$$\tau_w = \left( \frac{\partial U}{\partial Y} \right)_{y=0}, \theta_w = \left( \frac{\partial \theta}{\partial Y} \right)_{y=0}, \phi_w = \left( \frac{\partial \phi}{\partial Y} \right)_{y=0}. \quad (22)$$

#### 4. Results and Discussion

The current section is devoted to the physical behaviors of the material properties such as velocity distribution,  $U$ , temperature distribution,  $\theta$ , and mass concentration,  $\phi$ , under

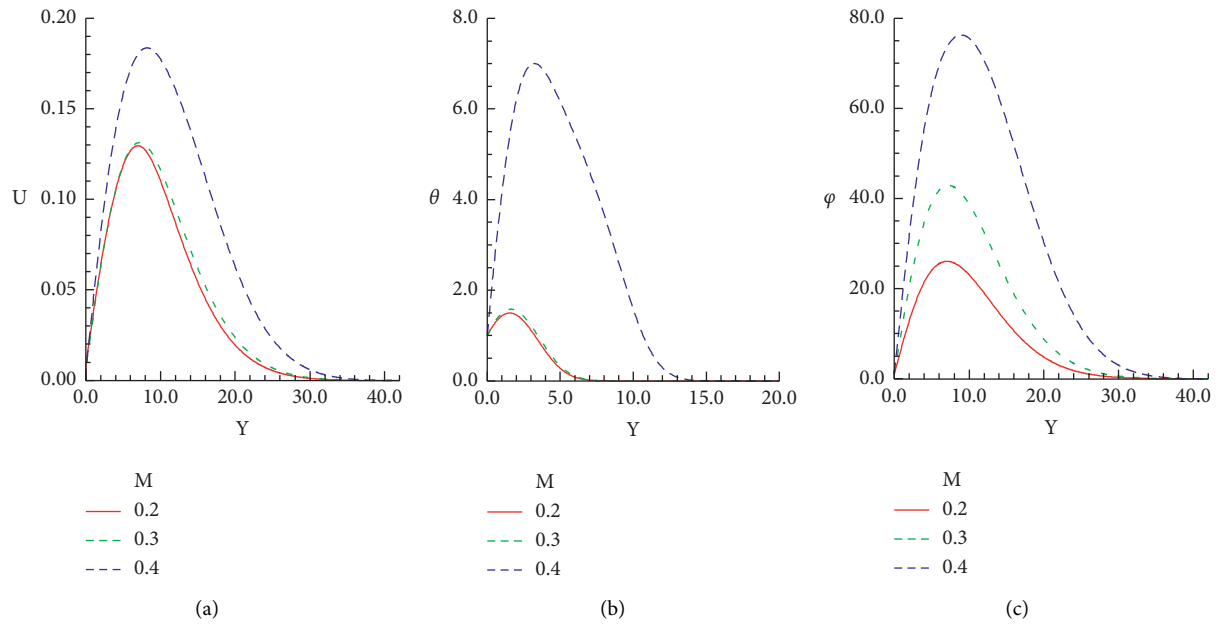


FIGURE 4: Plots for (a)  $U$ , (b)  $\theta$ , and (c)  $\phi$  for different choices of Hartmann number  $M$  when  $n = 0.3, Pr = 7.0, E = 0.8, \beta = 0.4, \gamma = 0.0001, Sc = 0.8$ , and  $\lambda = 0.5$ .

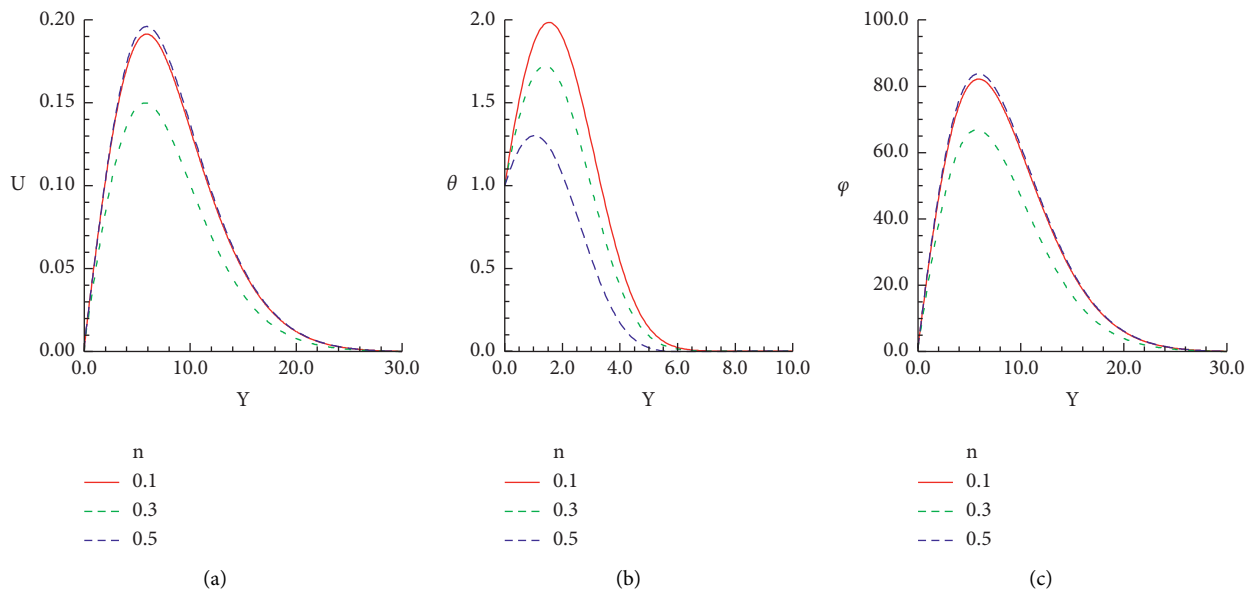


FIGURE 5: Plots for (a)  $U$ , (b)  $\theta$ , and (c)  $\phi$  for different choices of index number  $n$  when  $Sc = 0.8, Pr = 7.0, E = 0.4, \beta = 0.8, \gamma = 0.001, M = 0.4$ , and  $\lambda = 0$ .

the pertinent parameters. Also, the skin friction,  $\partial U/\partial Y$ , the rate of heat transfer,  $1/\partial Y$ , and the rate of mass transfer,  $\partial \phi/\partial Y$ , are taken into consideration under the same material parameters involved in the flow model. Figures 2(a)–2(c) show that the velocity profile, temperature distribution, and mass concentration show a prominent increase against the increasing values of  $Sc$  and the maximum values are observed for  $Sc = 0.2$ . From the graphical findings, it is concluded that all of three properties are satisfying the given boundary conditions and have shown very asymptotic behavior far

from the surface. Figures 3(a)–3(c) depict that the velocity, temperature distribution, and mass distributions decrease with increasing values of  $Pr$ . The above mechanism happens because, with an increase of the Prandtl number, the kinematic viscosity (or momentum diffusivity) increases, which slows down the motion. Also, the increasing  $Pr$  decreases the thermal conductivity which results in low-temperature distribution. The effect of varying  $M$  on velocity distribution, temperature distribution, and mass concentration are explained in Figures 4(a)–4(c). We observed that the fluid

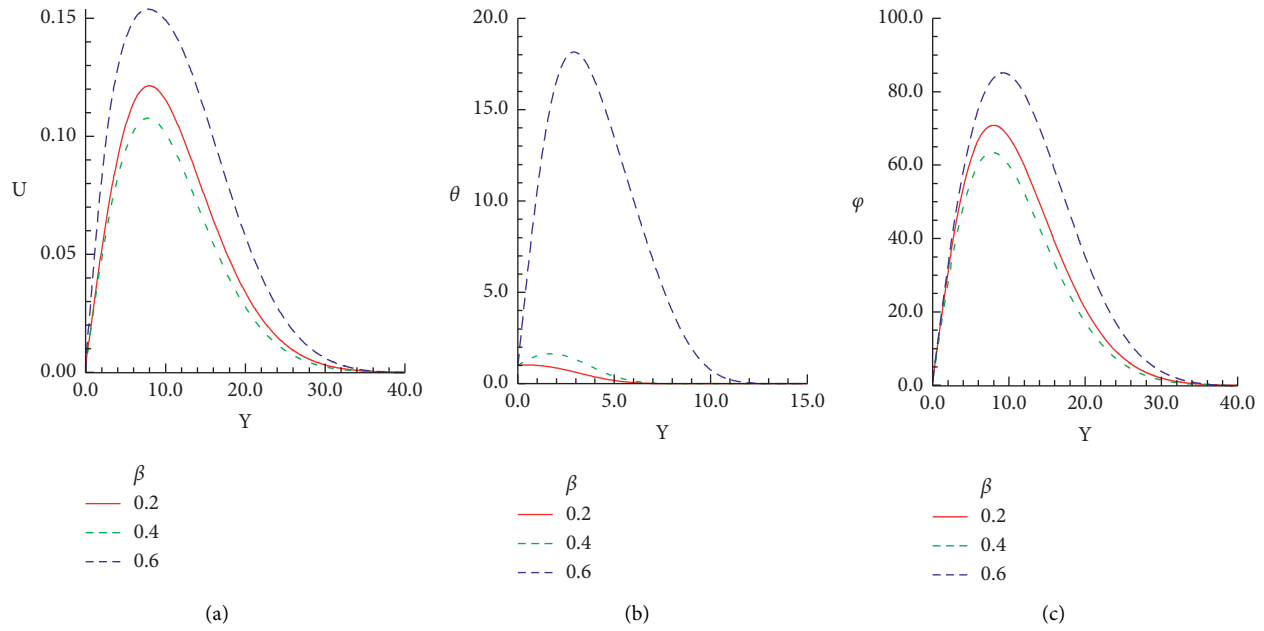


FIGURE 6: Plots for (a)  $U$ , (b)  $\theta$ , and (c)  $\phi$  for different choice of exothermic parameter  $\beta$  when  $n = 0.3$ ,  $Pr = 7.0$ ,  $E = 0.4$ ,  $Sc = 0.7$ ,  $\gamma = 0.0001$ ,  $M = 0.5$ , and  $\lambda = 0.4$ .

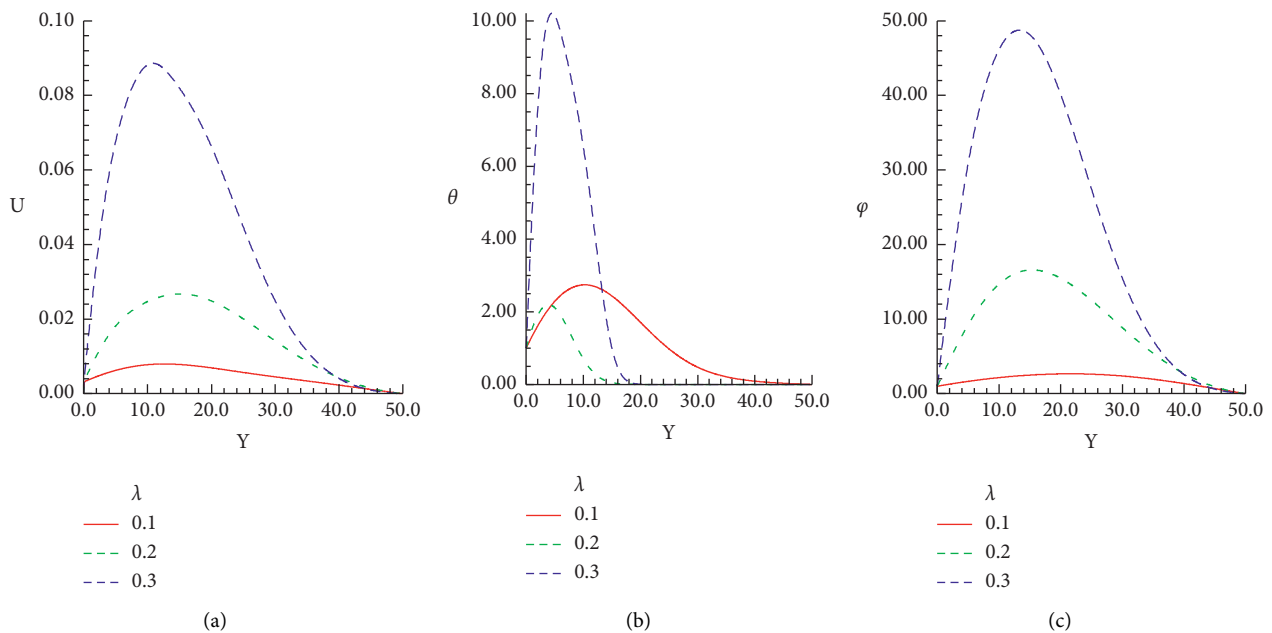


FIGURE 7: Plots for (a)  $U$ , (b)  $\theta$ , and (c)  $\phi$  for different choices of dimensionless chemical reaction rate constant  $\lambda$  when  $n = 0.3$ ,  $Pr = 7.0$ ,  $E = 0.4$ ,  $\beta = 0.5$ ,  $\gamma = 0.001$ ,  $M = 0.5$ , and  $Sc = 0.7$ .

properties  $U$ ,  $\theta$ , and  $\phi$  enhance simultaneously with an increase of  $M$ . It is significant to note that a slight change for velocity and temperature fields took place when  $M = 0.3$  and  $0.4$ , but a considerable increase in mass concentration with the increasing values of Hartmann number is noted.

Figures 5(a)–5(c) present the effect of different values of body shape parameter,  $n$ , on fluid velocity, temperature profile, and mass concentration. In these figures, we noted the trend that the velocity of the fluid flow domain and mass

concentration are maximum at  $n = 0.5$ , and for the same parametric condition, the temperature is decreased. The variation of exothermic parameter,  $\beta$ , on the velocity profile, temperature distribution, and mass concentration is flaunted in Figures 6(a)–6(c). From these figures, it is noted that, with the augmented values of  $\beta$ , the temperature distribution has extensively increased for  $\beta = 0.6$ , whereas the fluid velocity and the mass concentration demonstrate a considerable increase near the surface and approach to zero



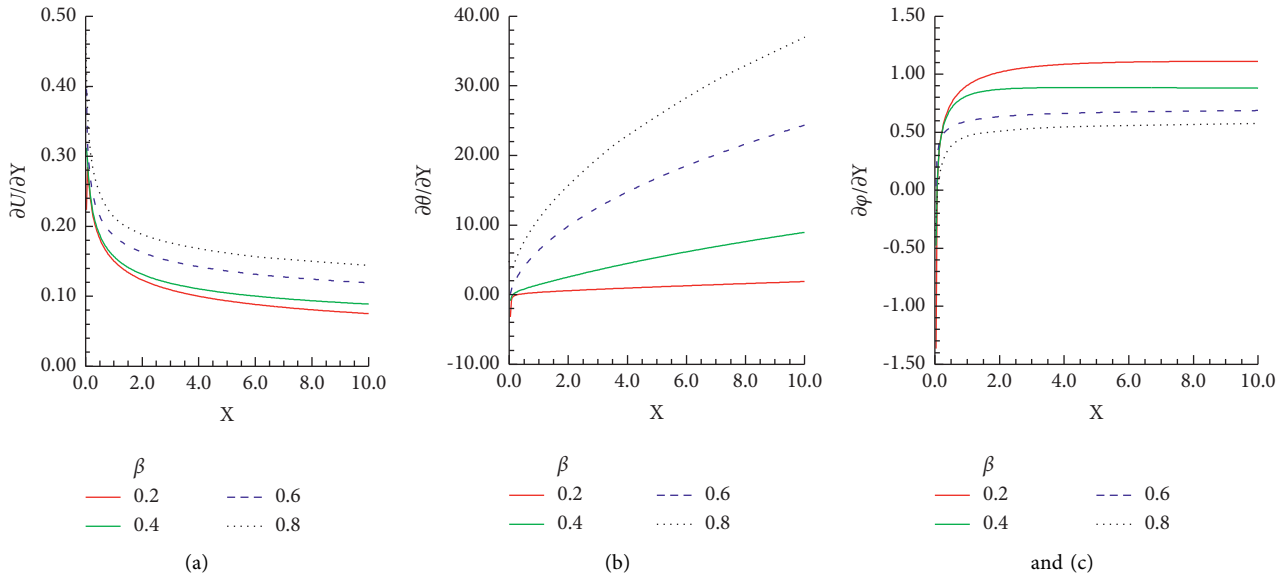


FIGURE 8: Plots for (a)  $\tau_w = (\partial U/\partial Y)_{y=0}$ , (b)  $\theta_w = (\partial \theta/\partial Y)_{y=0}$ , and (c)  $\phi_w = (\partial \phi/\partial Y)_{y=0}$  for various choices of exothermic parameter  $\beta$  when  $n = 0.3$ ,  $Pr = 7.0$ ,  $E = 0.4$ ,  $Sc = 0.8$ ,  $\gamma = 0.0001$ ,  $M = 0.4$ , and  $\lambda = 0.4$ .

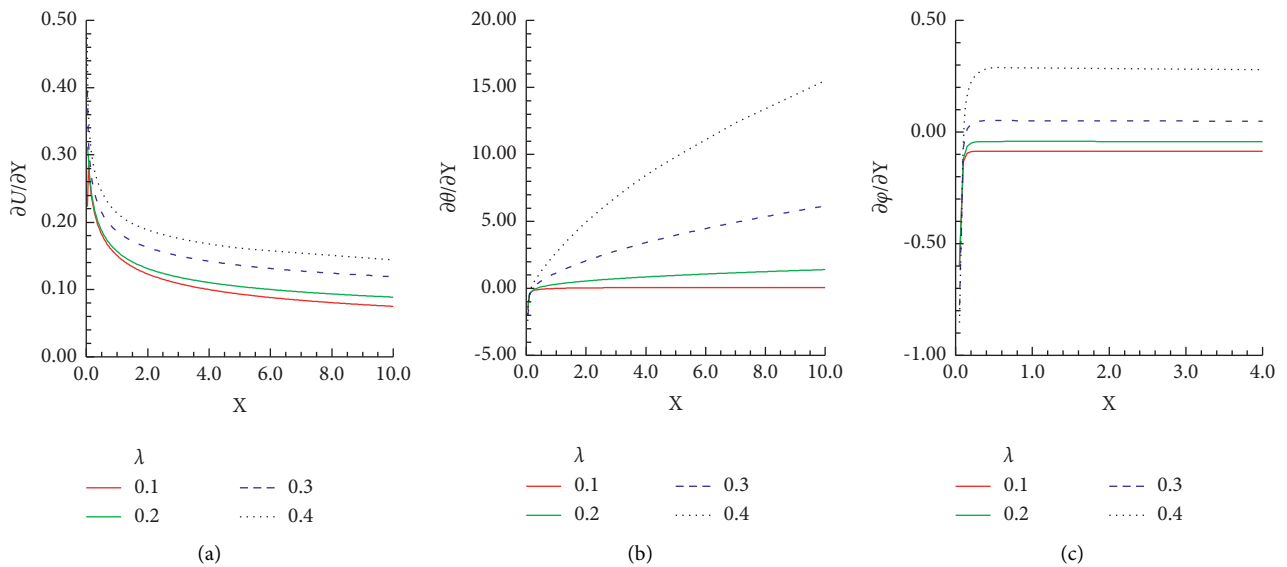


FIGURE 9: Plots for (a)  $\tau_w = (\partial U/\partial Y)_{y=0}$ , (b)  $\theta_w = (\partial \theta/\partial Y)_{y=0}$ , and (c)  $\phi_w = (\partial \phi/\partial Y)_{y=0}$ , for various choices of dimensionless chemical reaction rate  $\lambda$  when  $n = 0.3$ ,  $Pr = 7.0$ ,  $E = 0.4$ ,  $Sc = 0.6$ ,  $\gamma = 0.0001$ ,  $M = 0.4$ , and  $\beta = 0.5$ .

far from the surface. Graphical results showed that the boundary conditions are satisfied. Results reported in Figures 7(a)–7(c) are exploring the effect of increasing values of dimensionless chemical reaction rate constant  $\lambda$  on fluid velocity, temperature distribution, and mass concentration. From the observation of the flow patterns, it is concluded that the velocity profile, temperature distribution, and mass concentration mark an incredible increase with an increase in  $\lambda$ .

Now, in the preceding paragraph, we will converge our efforts to the interpretation of the results, particularly the effect of dimensionless numbers on local skin friction, the

rate of heat, and the mass transfer along the surface of body shape. Figures 8(a)–8(c) display the performance of  $\beta$  on the skin friction, heat, and mass flux. These figures illustrate that, with an increase in  $\beta$ , the physical property,  $\tau_w$ , has decreased, whereas  $\theta_w$  and  $\phi_w$  have increased. The behavior of  $\tau_w$ ,  $\theta_w$ , and  $\phi_w$  for dimensionless chemical reaction rate constant  $\lambda$  is analyzed in Figures 9(a)–9(c). From these sketches, it is noted that  $\tau_w$  is decreasing, but meanwhile,  $\theta_w$  and  $\phi_w$  are increasing for increasing values of  $\lambda$ . It is noteworthy in the case of the mass transfer rate that, after attaining its peak value at 0.25, the graph becomes constant for all values of  $\lambda$ . Figures 10(a)–10(c) represent the effect of

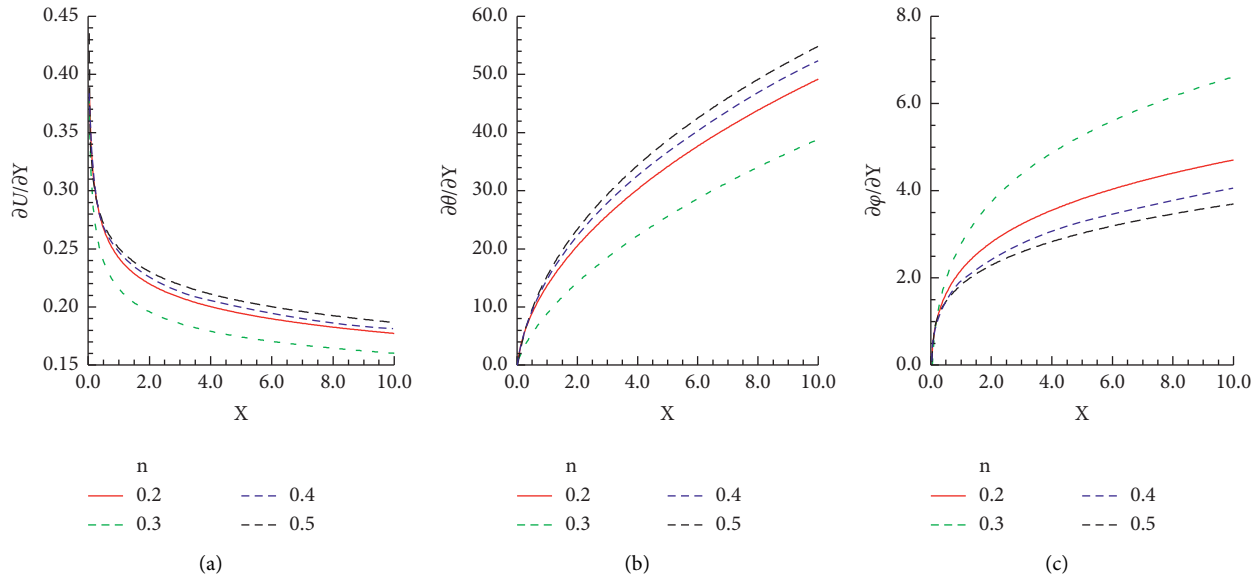


FIGURE 10: Plots for (a)  $\tau_w = (\partial U/\partial Y)_{y=0}$ , (b)  $\theta_w = (\partial \theta/\partial Y)_{y=0}$ , and (c)  $\phi_w = (\partial \phi/\partial Y)_{y=0}$ , for various choices of index parameter  $n$  when  $Pr = 7.0$ ,  $E = 0.4$ ,  $Sc = 0.6$ ,  $\gamma = 0.0001$ ,  $M = 0.4$ , and  $\beta =$ .

TABLE 1: The results of  $\tau_w = (\partial U/\partial Y)_{y=0}$ ,  $\theta_w = (\partial \theta/\partial Y)_{y=0}$ , and  $\phi_w = (\partial \phi/\partial Y)_{y=0}$  along different points of curved surface for different values of Prandtl number  $Pr$  by keeping  $n = 0.3$ ,  $Sc = 0.8$ ,  $E = 0.8$ ,  $\beta = 0.8$ ,  $\gamma = 0.0001$ ,  $M = 0.2$ , and  $\lambda = 0.5$ .

$X(m)$	$(\partial u/\partial y)_{y=0}$		$(\partial \theta/\partial y)_{y=0}$		$(\partial \phi/\partial y)_{y=0}$	
	$Pr = 0.71$	$Pr = 7.0$	$Pr = 0.71$	$Pr = 7.0$	$Pr = 0.71$	$Pr = 7.0$
0	0.46344	0.54678	0.34199	0.33971	0.34394	0.07316
1.0	0.22501	0.27335	0.27805	4.27181	0.69786	0.50550
2.0	0.18626	0.23807	0.31512	6.35778	0.89858	0.55505
3.0	0.16613	0.21970	0.32977	7.95343	1.01896	0.57828
4.0	0.15290	0.20750	0.33748	9.27855	1.10474	0.59220
5.0	0.14322	0.19844	0.34212	10.42374	1.17101	0.60154
6.0	0.13567	0.19126	0.34514	11.43726	1.22470	0.60819
7.0	0.12953	0.18533	0.34722	12.34851	1.26960	0.61312
8.0	0.12439	0.18027	0.34871	13.17694	1.30800	0.61685
9.0	0.11998	0.17587	0.34980	13.93617	1.34142	0.61972
10.0	0.11615	0.17197	0.35061	14.63614	1.37088	0.62193

varying  $n$  on  $\tau_w$ ,  $\theta_w$ , and  $\phi_w$ . In these plots, it is observed that, with the increase of  $n$ ,  $\tau_w$  has decreased whereas  $\theta_w$  and  $\phi_w$  have increased. The skin friction and the heat transfer rate have minimum value for  $n = 0.3$ , but the mass transfer rate represents its maximum magnitude for  $n = 0.3$ .

Table 1 presents skin friction, heat transfer, and mass transfer versus the distance  $X$  along the curved surface for  $Pr$  by taking two different values 0.71 and 7.0, i.e., for air and water. It is clearly observed that, with the increase of  $Pr$  on the skin, friction is increasing at the surface for different values of  $Pr$ , but it is also worth mentioning that the skin friction is decreasing downstream, whereas both heat and mass transfer rates show the opposite trend. They have increased along the surface and exhibit gradually decreasing behavior at the surface. In Table 2, it is noted that there is a mild decrease in the skin friction with enhancing values of  $M$  at the leading edge, and it also kept on decreasing along the surface. Since the Hartmann number is

the ratio of magnetic force to the inertial force, so with the increase of  $M$ , magnetic force increases, due to which electric current is generating in the fluid causing more the skin friction at the surface. It is also observed that, at the surface, heat transfer rate is increased with the increasing value of  $M$  and is also increasing along the surface. A completely different behavior is examined in the case of mass flux. It is increasing at the surface with the increasing values of  $M$  and has also increased downstream, but for  $M = 0.4$ , it descends at the beginning but then ascends very slowly beyond  $X = 4.0$ . For various values  $\gamma$ , the behavior of skin friction, heat transfer, and mass transfer is illustrated in Table 3. It is seen that there is a mild decrease in skin friction with increasing values of  $\gamma$  and that the skin friction is decreasing downstream. Apart from it, both the heat transfer rate and mass transfer rate have increased along the surface, but they have decreased gradually with the increasing values of  $\gamma$ .

TABLE 2: The results of  $\tau_w = (\partial U/\partial Y)_{y=0}$ ,  $\theta_w = (\partial \theta/\partial Y)_{y=0}$ , and  $\phi_w = (\partial \phi/\partial Y)_{y=0}$  along different points of the curved surface for different values of Hartmann number  $M$  by keeping  $n = 0.3$ ,  $Sc = 0.6$ ,  $E = 0.4$ ,  $\beta = 0.4$ ,  $\gamma = 0.00001$ ,  $Pr = 10.0$ , and  $\lambda = 0.5$ .

$X(m)$	$(\partial u/\partial y)_{y=0}$		$(\partial \theta/\partial y)_{y=0}$		$(\partial \phi/\partial y)_{y=0}$	
	$M = 0.2$	$M = 0.4$	$M = 0.2$	$M = 0.4$	$M = 0.2$	$M = 0.4$
0	0.50227	0.47482	1.24478	2.02307	0.17477	4.40132
1.0	0.25912	0.18578	2.86194	4.22762	0.90754	2.67263
2.0	0.21990	0.15804	3.87160	6.63239	1.18321	2.84959
3.0	0.19985	0.14471	4.69643	8.75057	1.33846	2.93221
4.0	0.18685	0.13642	5.42345	10.68653	1.44456	2.98226
5.0	0.17743	0.13059	6.08551	12.48254	1.52403	3.01680
6.0	0.17015	0.12616	6.69952	14.16367	1.58690	3.04258
7.0	0.16427	0.12265	7.27566	15.74751	1.63850	3.06285
8.0	0.15937	0.11975	7.82067	17.24738	1.68199	3.07938
9.0	0.15519	0.11729	8.33933	18.67383	1.71938	3.09323
10.0	0.15157	0.11517	8.83519	20.03539	1.75204	3.10508

TABLE 3: The results of  $\tau_w = (\partial U/\partial Y)_{y=0}$ ,  $\theta_w = (\partial \theta/\partial Y)_{y=0}$ , and  $\phi_w = (\partial \phi/\partial Y)_{y=0}$  along different points of the curved surface for different values of temperature relative parameter  $\gamma$  by keeping  $n = 0.3$ ,  $Sc = 0.6$ ,  $E = 0.4$ ,  $\beta = 0.5$ ,  $M = 0.4$ ,  $Pr = 10.0$ , and  $\lambda = 0.4$ .

$X(m)$	$(\partial u/\partial y)_{y=0}$		$(\partial \theta/\partial y)_{y=0}$		$(\partial \phi/\partial y)_{y=0}$	
	$\gamma = 0.03$	$\gamma = 0.04$	$\gamma = 0.03$	$\gamma = 0.04$	$\gamma = 0.03$	$\gamma = 0.04$
1.0	0.17913	0.16003	5.45974	2.44013	0.37327	0.34846
2.0	0.15822	0.14117	9.08715	5.26400	0.42798	0.41146
3.0	0.14830	0.13301	12.19135	7.97995	0.47278	0.47138
4.0	0.14232	0.12852	15.15791	10.62013	0.51491	0.52922
5.0	0.13829	0.12583	17.67864	13.21581	0.55041	0.58577
6.0	0.13543	0.12418	20.21509	15.78696	0.58596	0.64158
7.0	0.13332	0.12322	22.66189	18.34633	0.62016	0.69703
8.0	0.13172	0.12272	25.03919	20.90237	0.65331	0.75236
9.0	0.13051	0.12256	27.36083	23.46087	0.68566	0.80775
10.0	0.12958	0.12266	26.63683	26.02594	0.71736	0.86333

### 5. Concluding Remarks

The problem of natural convection flow is carried out in a curved surface along with exothermic catalytic chemical reaction, and a magnetic field is investigated by different physiological parameters. It is noteworthy that, by increasing the Schmidt number  $Sc$ , velocity field, temperature profile, and mass concentration have increased, although, an increase in  $Pr$  has reduced the field fluid velocity, temperature profile, and maximum concentration. With the shear size of the Prandtl number, skin bumps are perceived to be rejected and temperature and mass transfer are increased. The size of the speed field, the distribution of temperature, and the concentration of weight are greatly enhanced by the high values of the Hartmann number which we have seen the skin collision decrease due to the increasing number of Hartmann numbers and away from the surface the impact of the magnetic field becomes much smaller. With increasing value  $\beta$ , the speed and concentration of the mass are determined by the magnitude, and the reverse behavior is observed in the case of temperature distribution. With a

wide range of body shape parameters  $n$ , skin friction and heat transfer are noted as improved but weight transfer decreases. Due to the increasing number of exothermic parameters, the fluid velocity and concentration are gradually reduced and the temperature distribution increases dramatically, which satisfies the boundary condition. Skin tension decreases while heat and bulk transfer increases above the rising values in the fluid velocity; the distribution of temperature and the concentration of the weight is greatly increased by a very high rate of noninvasive chemical reaction rate. The various impact of the temperature-related parameter reduces skin friction, heat transfer, and mass transfer freely over the surface. Moreover, from the systematic variation of the control parameters, the convective stability of the numerical solution is achieved using a finite difference method. The future work of the current study can be extended as

- (i) Magneto-exothermic catalytic chemical reaction along a truncated wavy cone
- (ii) Magneto-exothermic catalytic chemical reaction along a circular cylinder
- (iii) Magneto-exothermic catalytic chemical reaction along a spherical shell

### Abbreviations

- $n$ : Index parameter
- $Pr$ : Prandtl number
- $Sc$ : Schmidt number
- $u$ : Dimensionless velocity along  $x$  direction
- $v$ : Dimensionless velocity along  $y$  direction
- $x$ : Dimensionless distance along the surface
- $y$ : Dimensionless distance normal to the surface
- $T$ : Dimensioned surface temperature
- $T_{\infty}$ : Ambient temperature
- $E$ : Dimensionless activation energy
- $M$ : Hartmann number
- $\phi$ : Dimensionless temperature
- $\varnothing$ : Dimensionless mass concentration
- $\beta$ : Exothermic parameter
- $\gamma$ : Temperature relative parameter
- $\lambda$ : Chemical reaction rate constant.

### Data Availability

No data were used to support this study.

### Conflicts of Interest

The authors declare that they have no conflicts of interest.

### References

- [1] E. R. D'sa, "Magneto-hydrodynamic free convection in a strong cross-field," *Journal of Applied Mathematics and Physics(ZAMP)*, vol. 18, no. 1, pp. 106–115, 1976.
- [2] H. K. Kuiken, "Magneto-hydrodynamic free convection in a strong cross field," *Journal of Fluid Mechanics*, vol. 40, no. 01, pp. 21–38, 1970.

- [3] M. A. Hossain, K. C. A. Alam, and D. A. S. Rees, "MHD forced and free convection boundary layer flow along a vertical porous plate," *International Journal of Applied Mechanics and Engineering*, vol. 2, no. 1, pp. 33–51, 1997.
- [4] A. A. Afify, "MHD free convection flow and mass transfer over a stretching sheet with chemical reaction," *Journal of Heat and Mass Transfer*, vol. 40, no. 6, pp. 495–500, 2004.
- [5] O. D. Makinde and A. Aziz, "MHD mixed convection from a vertical plate embedded in a porous medium with a convective boundary condition," *International Journal of Thermal Sciences*, vol. 49, no. 9, pp. 1813–1820, 2010.
- [6] Z. Stamenkovic, D. Nikodijevic, M. Kocic, and J. Nikodijevic, "Mhd flow and heat transfer of two immiscible fluids with induced magnetic field effects," *Thermal Science*, vol. 16, no. suppl. 2, pp. 323–336, 2012.
- [7] M. Ashraf, S. Asghar, and M. A. Hossain, "Computational study of combined effects of conduction-radiation and hydromagnetics on natural convection flow past magnetized permeable plate," *Applied Mathematics and Mechanics*, vol. 33, no. 6, pp. 731–748, 2012.
- [8] L. Rongy, P. Assemat, and A. De Wit, "Marangoni-driven convection around exothermic autocatalytic chemical fronts in free-surface solution layers," *Chaos: An Interdisciplinary Journal of Nonlinear Science*, vol. 22, no. 3, Article ID 037106, 2012.
- [9] B. R. Rout, S. K. Parida, and S. Panda, "MHD heat and mass transfer of chemical reaction fluid flow over a moving vertical plate in presence of heat source with convective surface boundary condition," *International Journal of Chemical Engineering*, vol. 5, 2013.
- [10] K. A. Maleque, "Effects of exothermic/endothemic chemical reactions with Arrhenius activation energy on MHD free convection and mass transfer flow in presence of thermal radiation," *Journal of Thermodynamics*, vol. 2013, pp. 1–11, 2013.
- [11] K. A. Maleque, "Effects of binary chemical reaction and activation energy on MHD boundary layer heat and mass transfer flow with viscous dissipation and heat generation/absorption," *ISRN Thermodynamics*, vol. 2013, pp. 1–9, 2013.
- [12] C. Jayabalan, K. K. Sivagnana Prabhu, and R. Kandasamy, "Heat enhanced by an exothermic reaction on a fully developed MHD mixed convection flow in a vertical channel," *Journal of Applied Mechanics and Technical Physics*, vol. 57, no. 5, pp. 957–962, 2016.
- [13] M. Ashraf, A. J. Chamkha, S. Iqbal, and M. Ahmad, "Effects of temperature-dependent viscosity and thermal conductivity on mixed convection flow along a magnetized vertical surface," *International Journal of Numerical Methods for Heat and Fluid Flow*, vol. 5, pp. 1580–1592, 2017.
- [14] M. S. Anwar and A. Rasheed, "Heat transfer at microscopic level in a MHD fractional inertial flow confined between non-isothermal boundaries," *European Physical Journal Plus*, vol. 132, no. 305S, 2017.
- [15] A. Rasheed and M. S. Anwar, "Joule heating in magnetic resistive flow with fractional Cattaneo–Maxwell model," *Journal of the Brazilian Society of Mechanical Sciences and Engineering*, pp. 44–501, 2018.
- [16] Y. S. Daniel, Z. A. Aziz, Z. Ismail, and F. Salah, "Thermal stratification effects on MHD radiative flow of nanofluid over nonlinear stretching sheet with variable thickness," *Journal of Computational Design and Engineering*, vol. 5, no. 2, pp. 232–242, 2018.
- [17] M. M. Hamza, "Free convection slip flow of an exothermic fluid in a convectively heated vertical channel," *Ain Shams Engineering Journal*, vol. 9, no. 4, pp. 1313–1323, 2018.
- [18] M. Ashraf, U. Ahmad, and A. J. Chamkha, "Computational analysis of natural convection flow driven along a curved surface in the presence of exothermic catalytic chemical reaction," *Computational Thermal Sciences: International Journal*, vol. 11, no. 4, pp. 339–351, 2019.